Available online at www.sciencedirect.com

ScienceDirect

Mendeleev Commun., 2024, **34**, 226–228

Mendeleev Communications

Observing the formation of TiO_2 mesocrystals from NH_4TiOF_3 microparticles using *in situ* thermo-WAXS measurements

Alexey A. Sadovnikov*[a,b] and Olga V. Boytsova*[c,d]

[a] *N. S. Kurnakov Institute of General and Inorganic Chemistry, Russian Academy of Sciences, 1199991 Moscow, Russian Federation. E-mail: trinki13@gmail.com*

[b] *A. V. Topchiev Institute of Petrochemical Synthesis, Russian Academy of Sciences, 119991 Moscow, Russian Federation*

[c] *Department of Materials Science, M. V. Lomonosov Moscow State University, 119991 Moscow, Russian Federation. E-mail: boytsova@gmail.com*

[d] *Department of Chemistry, M. V. Lomonosov Moscow State University, 119991 Moscow, Russian Federation*

DOI: 10.1016/j.mencom.2024.02.022

Real-time *in situ* X-ray analysis was used to shed light on the topotactic transformation of NH_4TiOF_3 into nanostructured TiO_2 mesocrystals. Specifically, for the system formed in the presence of the PEG-2000 templating polymer, XRD analysis showed that the overall transformation occurs through four separate transitions, consistent with previous reports. The applicability of synchrotron wide-angle X-ray scattering (WAXS) to real-time *in situ* analysis has enabled precise temperature mapping of these four transitions and the identification of stability boundaries for the first time.

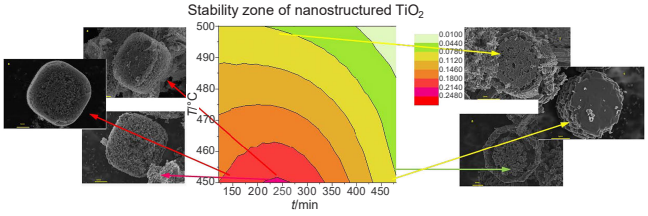

Keywords: anatase, TiO_2, mesocrystal, composites, WAXS, NH_4TiOF_3.

Mesocrystals are crystallographically ordered arrays of nanoparticles. Consequently, micron-sized mesocrystals can still exhibit the properties inherent in their constituent nanoparticles.[1–3] Titanium dioxide mesocrystals have been widely studied in many energy and environmental fields such as solar cells,[4] photocatalysis[5–8] and lithium-ion batteries.[9,10] This interest is due to their high chemical stability, non-toxicity, low cost, elemental content and unique physicochemical properties. As a result, significant progress has been made in the controlled synthesis of TiO_2 nanomaterials with tunable compositions, phases, sizes, shapes and architectures, since these parameters can significantly influence the properties of TiO_2 nanomaterials.[11–15] In particular, anatase TiO_2 nanosheets with highly active {001} facets have attracted considerable attention as they usually exhibit improved photocatalytic properties.[16] In addition, TiO_2 nanosheets with exposed {001} facets, combined into sandwich layers or mesocrystals with a similar structure, enable such materials to have excellent lithium-ion storage performance.[17] Interestingly, for systems in which ordered arrays of anatase nanocrystals are obtained by topotactic transformation from ammonium oxofluorotitanate, the boundaries of the stable state, *i.e.*, a state in which crystallite growth is possible only in the {001} direction, have not yet been reported.[18,19]

Here, we report a facile method to synthesize mesocrystals of TiO_2 nanosheets with dominant {001} facets and present X-ray diffraction (XRD) data on the mechanism of topotactic transformation of NH_4TiOF_3 to TiO_2 and the influence of annealing parameters on the properties of the resulting mesocrystals. Most notably, for ordered arrays of anatase nanocrystals, obtained from NH_4TiOF_3 mesocrystals formed in the presence of a PEG-2000 template, we determined regions of a stable mesostate and conditions for further growth of titanium dioxide nanoparticles inside the Type I mesocrystals.[20] Thus, mapping the stability of ordered arrays of anatase nanocrystals made it possible to predict the conditions for the synthesis of the most effective nanophotocatalyst in particular and functional orientation-sensitive nanomaterials in the form of mesocrystals in general (see Online Supplementary Materials). This knowledge could be useful for generating mesocrystalline materials consisting of arrays of one or more types of nanoparticles, with specific properties configured to enable their use in practical applications of mesocrystals or any metamaterials.

A sample of NH_4TiOF_3 mesocrystals was synthesized in the presence of PEG-2000 using a previously described synthetic procedure.[21] This protocol results in the formation of micron-sized NH_4TiOF_3 particles of a specific shape, separated from each other by a polymer additive, in this case PEG-2000. When analyzed by XRD, this sample showed a typical XRD pattern of NH_4TiOF_3 [Figure 1(*a*)], having lattice parameters $a = 7.5526(1)$ Å, $b = 6.3051(1)$ Å and $c = 7.5845(1)$ Å.[21] The scanning electron microscopy (SEM) images show that the NH_4TiOF_3 microparticles have the shape of a regular rectangular prism with a length/width of about 4 μm and a height varying in the range of approximately 1.7–2.0 μm [Figure 1(*b*),(*c*)].

Understanding where the boundaries of stability of intermediate nanoparticles lie during the transformation of NH_4TiOF_3 into titanium dioxide mesocrystals is a key. To determine the stability boundaries for the conversion of NH_4TiOF_3 into ordered arrays of TiO_2 nanocrystals, we performed thermogravimetric analysis (TGA) [Figure 1(*d*)] and differential thermal analysis (DTA)

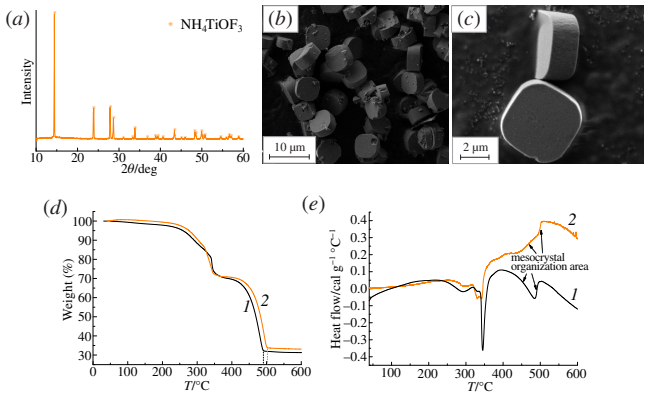

Figure 1 (*a*) XRD pattern of NH_4TiOF_3. (*b*),(*c*) SEM micrographs of NH_4TiOF_3 mesocrystals formed in the presence of PEG-2000. (*d*) TGA and (*e*) DTA curves of NH_4TiOF_3 in (*1*) an air atmosphere and (*2*) an argon atmosphere. Arrows indicate mesocrystal generation zone.

[Figure 1(*e*)] both in air (curve *1*) and in an argon atmosphere (curve *2*). In both cases, four different stages were observed, which is consistent with previous research.[22,23] When heated in air in the first stage (25–230 °C), water and other volatile components are removed [reaction (1)]. At the second stage (230–340 °C), the conversion of NH_4TiOF_3 to $HTiOF_3$ occurs with the loss of NH_3 [reaction (2)]. The third stage (340–380 °C) corresponds to the transition of $HTiOF_3$ into $TiOF_2$ with the concomitant loss of HF from the mixture (absorption of fluoride by boric acid) [reaction (3)]. At the final fourth stage (380–480 °C) $TiOF_2$ is converted into TiO_2 [reaction (4)].

$$NH_4TiOF_3 \cdot H_2O_{sorb} = NH_4TiOF_3 + H_2O_{sorb}\uparrow \quad (1)$$

$$NH_4TiOF_3 = HTiOF_3 + NH_3\uparrow \quad (2)$$

$$HTiOF_3 = TiOF_2 + HF\uparrow \quad (3)$$

$$TiOF_2 + H_2O = TiO_2 + 2HF \quad (4)$$

Conversion processes in the temperature ranges of 380–480 °C in air and 380–510 °C in argon, associated with the transition from $TiOF_2$ to TiO_2, shows differences in stability limits. Oxygen in the air can accelerate the final stage of decomposition. Thus, when NH_4TiOF_3 is heated in air for two and four hours at a temperature of 450 °C, lozenge-shaped TiO_2 mesocrystals are formed [Figure 2(*a*),(*b*)]. In stark contrast, annealing an identical NH_4TiOF_3 sample in air at a temperature of 500 °C leads to the destruction of mesocrystals and the formation of individual nanocrystals of titanium dioxide, which

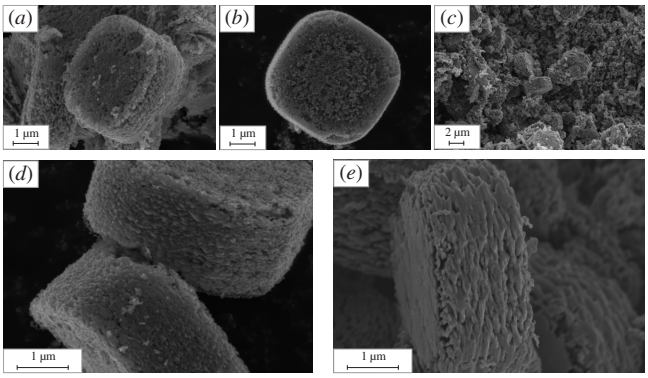

Figure 2 SEM images of (*a*)–(*c*) ordered arrays of TiO_2 nanocrystals and (*d*),(*e*) TiO_2 mesocrystals with thicknesses of (*d*) ~1.90 and (*e*) ~1.66 μm obtained from (*a*)–(*c*) random or (*d*),(*e*) identical NH_4TiOF_3 samples by annealing in (*a*)–(*d*) air and (*e*) argon at (*a*),(*b*),(*d*),(*e*) 450 and (*c*) 500 °C for (*a*),(*c*) 2 and (*b*),(*d*),(*e*) 4 h. For additional SEM images, see Figure S6 in Online Supplementary Materials.

Table 1 Main characteristics of samples of ordered arrays of TiO_2 nanocrystals obtained by annealing NH_4TiOF_3 mesocrystals.

Sample	Annealing conditions			Crystallite size (by XRD)/nm
	Atmosphere	*t*/h	*T*/°C	
450_2	Air	2	450	40 ± 2
450_4	Air	4	450	37 ± 2
450_8	Air	8	450	44 ± 4
500_2	Air	2	500	42 ± 2
500_4	Air	4	500	45 ± 3
500_8	Air	8	500	–[a]
450_2_Ar	Ar	2	450	47 ± 2
450_4_Ar	Ar	4	450	40 ± 2
450_8_Ar	Ar	8	450	43 ± 4
500_2_Ar	Ar	2	500	44 ± 2
500_4_Ar	Ar	4	500	46 ± 3
500_8_Ar	Ar	8	500	–[a]

[a] No mesocrystals formed.

is confirmed by SEM [Figure 2(*c*)]. Moreover, the duration of annealing at a certain temperature affects the size of titanium dioxide crystallites (Table 1).

Thermal XRD data are in satisfactory agreement with the TGA data and confirm the above scheme of reactions (1)–(4) for the conversion of NH_4TiOF_3 to TiO_2. The final powders obtained are single-phase and have an anatase structure (Figures S1 and S2, see Online Supplementary Materials). The lattice parameters of TiO_2 were estimated to be $a = 3.793$ Å and $c = 9.485$ Å, which is in excellent agreement with the published data.[24] The mesocrystallinity and high-order orientation of the nanoparticles composing the TiO_2 mesocrystals were confirmed by SEM (Figure S3), transmission electron microscopy (TEM) (Figure S4) and selected area electron diffraction (SAED) (Figure S4). Moreover, TEM and SAED data confirmed the 001-directed growth of TiO_2 mesocrystals formed from NH_4TiOF_3 single crystals that were prepared in the presence of the PEG-2000 template (Figure S4). The single-crystal diffraction pattern obtained for one of these TiO_2 mesocrystals is consistent with that previously reported for Type I mesocrystals.[25]

Inspired by such well-defined reaction steps as evidenced by TGA and XRD, we sought to shed further light on these transitions by conducting a series of real-time XRD studies. Specifically, NH_4TiOF_3 samples were subjected to annealing at temperatures up to 600 °C in air, and real-time XRD patterns were recorded during heating. Clear structural changes can be seen in four different temperature ranges (Figure 3). These are consistent with an initial reversible phase transition of NH_4TiOF_3 ($Pca2_1$ to $Pma2$) at about 180 °C, as described in our recent

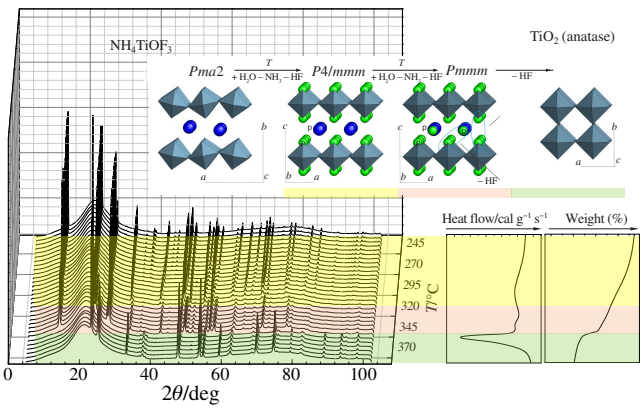

Figure 3 Superimposed *in situ* XRD patterns of an NH_4TiOF_3 sample gradually heated from 225 to 385 °C in air. The heat flow to the sample and the weight loss from it under the same conditions are shown in the inset on the right.

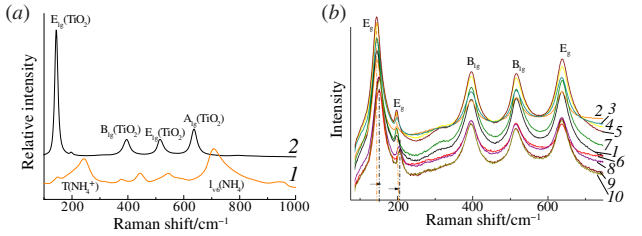

Figure 4 (*a*) Raman spectra of (*1*) NH_4TiOF_3 before annealing and (*2*) anatase TiO_2 obtained by annealing NH_4TiOF_3 in air at 450 °C for 2 h. (*b*) Raman spectra of TiO_2 mesocrystal samples prepared by heating NH_4TiOF_3 mesocrystals in (*1*)–(*5*) air and (*6*)–(*10*) argon at (*1*)–(*3*),(*6*)–(*8*) 450 and (*4*),(*5*),(*9*),(*10*) 500 °C for (*1*),(*4*),(*6*),(*9*) 2, (*2*),(*5*),(*7*),(*10*) 4 and (*3*),(*8*) 8 h. Two arrows indicate the shifts of the E_g signals when heating was carried out in an argon atmosphere.

work,[21] followed by three structural transitions in the temperature range 225–385 °C. These transitions are brought about by three distinct chemical reactions (2)–(4) as NH_4TiOF_3 is converted to TiO_2 by the action of heat. It is notable that these structural/chemical transitions occur at very specific temperatures and that real-time *in situ* XRD can accurately measure these temperatures (Figures 3 and S5).

All samples were investigated by Raman spectroscopy [Figure 4(*a*),(*b*)]. The spectra of the annealed samples demonstrate only anatase reflections [Figure 4(*b*)].[26] In the spectra of samples annealed in an argon atmosphere, shifts of the E_g lines at 100 and 200 cm^{-1} are observed, while the remaining lines do not change their positions. The shift in the E_g line of TiO_2 may be associated with a change in particle size in the lateral direction, which likely reflects a change in the mechanism of thermally mediated transition from NH_4TiOF_3 to TiO_2 and a concomitant increase in the volume of TiO_2 nanoparticles that make up the TiO_2 mesocrystal. The change in nanoparticle growth is consistent with SEM data [Figure 2(*d*),(*e*)]. This is consistent with SEM and XRD data, according to which, when the annealing temperature changes from 450 to 500 °C, the stabilization of the dioxide mesocrystal by the polymer is impaired and the isotropic growth of titanium dioxide crystallites begins. This transition from nonclassical to more classical growth probably leads to a decrease in the area of photoactive {001} planes.

In more specific comparative analyses, it was shown, mainly by SEM, that with increasing annealing temperature from 450 to 500 °C in an argon atmosphere, the ordering of crystallites in the layers is completely destroyed, although in general overall structural terms the mesocrystals largely retain their overall structural integrity (Figure S7). Among other changes that occurred, the thickness of the ordered arrays of TiO_2 nanocrystals changed from 1.2 ± 0.2 μm to 1.4 ± 0.2 μm upon annealing at 450 and 500 °C, respectively.

In summary, three factors that affect the formation of nanostructured TiO_2 photocatalyst from NH_4TiOF_3 mesocrystal precursors were evaluated: annealing temperature, annealing time and annealing atmosphere. TGA and X-ray phase analysis data made it possible to establish the stability limits of anatase mesocrystals obtained from ammonium oxofluorotitanate. These observations were complemented by SEM analysis, and together these data allowed us to determine the influence of processing parameters (annealing temperature, time and atmosphere) on the boundaries of formation of stable titanium dioxide mesocrystals. Our results have more general implications as they are likely to be applicable to nanoparticle arrays generated in other mesocrystal-forming reaction systems, where a range of variable reaction conditions and parameters are used to produce nanostructured mesocrystals for the desired application. Reconstruction of the stability map of mesocrystals makes it possible to predict the conditions for the synthesis, in particular, of a highly efficient nanophotocatalyst for water splitting.

We thank Dr. Chernyshov and Dr. Bosak for assistance with diffraction measurements on the BM01 SNBL and ID28 beamlines at ESRF. SEM analysis was carried out using the equipment of the JRC PMR IGIC RAS. O.V.B. acknowledges the financial support from the Russian Science Foundation (grant no. 22-29-00963).

Online Supplementary Materials

Supplementary data associated with this article can be found in the online version at doi: 10.1016/j.mencom.2024.02.022.

References

1 E. V. Sturm and H. Cölfen, *Crystals*, 2017, **7**, 207.
2 D. Yang, W. Zhang, Y. Wang, L. Li, F. Yao, L. Miao, W. Zhao, X. Kong, Q. Feng and D. Hu, *Ceram. Int.*, 2021, **47**, 1479.
3 D. Egea-Benavente, C. Díaz-Ufano, Á. Gallo-Cordova, F. J. Palomares, J. L. Cuya Huaman, D. F. Barber, M. del Puerto Morales and J. Balachandran, *ACS Appl. Mater. Interfaces*, 2023, **15**, 32162.
4 D. Wu, K. Cao, H. Wang, F. Wang, Z. Gao, F. Xu, Y. Guo and K. Jiang, *J. Colloid Interface Sci.*, 2015, **456**, 125.
5 Y. Guo, H. Li, J. Chen, X. Wu and L. Zhou, *J. Mater. Chem. A*, 2014, **2**, 19589.
6 H. Li and Z. Su, *J. Colloid Interface Sci.*, 2022, **617**, 267.
7 M. V. Korolenko, P. B. Fabritchnyi and M. I. Afanasov, *Mendeleev Commun.*, 2023, **33**, 133.
8 M. V. Korolenko, P. B. Fabritchnyi and M. I. Afanasov, *Mendeleev Commun*., 2023, **33**, 864.
9 Z. Hong, M. Wei, T. Lan and G. Cao, *Nano Energy*, 2012, **1**, 466.
10 W. Zhang, J. Wu, Y. Li, X. Feng, L. Wang, X. He, N.-L. Wu, M. Ouyang and M. Wei, *J. Colloid Interface Sci.*, 2022, **625**, 692.
11 A. A. Sadovnikov, A. V. Garshev, A. A. Eliseev, A. N. Beltiukov, E. R. Naranov, W. Li, A. J. Sutherland and O. V. Boytsova, *Catal. Today*, 2021, **378,** 133.
12 Y. Murakami, T. Kamegawa, Y. Kobori and T. Tachikawa, *Nanoscale*, 2020, **12**, 6420.
13 A. N. El-Shazly, G. S. El-Sayyad, A. H. Hegazy, M. A. Hamza, R. M. Fathy, E. T. El Shenawy and N. K. Allam, *Sci. Rep.*, 2021, **11,** 5609.
14 M. Guo, D. Shen, Y. Li, M. A. Akram and M. Wei, *ChemSusChem*, 2020, **13**, 5256.
15 M. H. Razali and M. Yusoff, *Mater. Lett.*, 2018, **221**, 168.
16 Y.-H. Wu, Y.-N. Lu, L.-J. Ma, H. Chen, Y.-X. Wang, W.-Q. Wu, B.-X. Lei and Z.-F. Sun, *J. Phys. Chem. C*, 2021, **125**, 1684.
17 O. V. Boytsova, O. A. Drozhzhin, D. I. Petukhov, A. V. Chumakova, A. G. Sobol, A. N. Beltyukov, A. A. Eliseev and A. B. Bosak, *Nanotechnology*, 2022, **33**, 055603.
18 M. Inoguchi, M. Afzaal, N. Tanaka and P. O'Brien, *J. Mater. Chem.*, 2012, **22**, 25123.
19 B. Lei, Y. Guo, H. Xie, J. Chen, X. Li, Y. Wu and L. Zhou, *Cryst. Growth Des.*, 2019, **19**, 5460.
20 C. Liu, Z. Ou, S. Zhou and Q. Chen, in *Crystallization via Nonclassical Pathways*, ed. X. Zhang, American Chemical Society, Washington, DC, 2020, vol. 1, pp. 115–146, DOI: 10.1021/bk-2020-1358.ch006.
21 O. Boytsova, I. Dovgaliuk, D. Chernyshov, A. Eliseev, P. O'Brien, A. J. Sutherland and A. Bosak, *J. Appl. Crystallogr.*, 2019, **52**, 23.
22 L. Zhou, D. Smyth-Boyle and P. O'Brien, *J. Am. Chem. Soc.*, 2008, **130**, 1309.
23 O. Boytsova, I. Zhukova, A. Tatarenko, T. Shatalova, A. Beiltiukov, A. Eliseev and A. Sadovnikov, *Nanomaterials*, 2022, **12**, 4418.
24 O. V. Boytsova, A. A. Sadovnikov, K. E. Yorov, A. N. Beltiukov, A. E. Baranchikov, V. K. Ivanov, X. Zhong, D. J. Lewis, P. O'Brien and A. J. Sutherland, *CrystEngComm*, 2017, **19**, 3281.
25 J. Brunner and H. Cölfen, in *Crystallization via Nonclassical Pathways*, ed. X. Zhang, American Chemical Society, Washington, DC, 2020, vol. 1, pp. 73–96, DOI: 10.1021/bk-2020-1358.ch004.
26 S. Balaji, Y. Djaoued and J. Robichaud, *J. Raman Spectrosc.*, 2006, **37**, 1416.

Received: 8th November 2023; Com. 23/7296